

---

This is an electronic reprint of the original article.  
This reprint may differ from the original in pagination and typographic detail.

Chen, Min; Avarmaa, Katri; Taskinen, Pekka; Klemettinen, Lassi; Michallik, Radoslaw;  
O'Brien, Hugh; Jokilaakso, Ari

## Novel fluxing strategy of copper matte smelting and trace metals in E-Waste recycling

*Published in:*  
Minerals Engineering

*DOI:*  
[10.1016/j.mineng.2022.107969](https://doi.org/10.1016/j.mineng.2022.107969)

Published: 01/01/2023

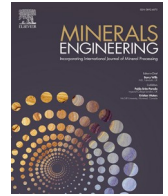
*Document Version*  
Publisher's PDF, also known as Version of record

*Published under the following license:*  
CC BY

*Please cite the original version:*  
Chen, M., Avarmaa, K., Taskinen, P., Klemettinen, L., Michallik, R., O'Brien, H., & Jokilaakso, A. (2023). Novel fluxing strategy of copper matte smelting and trace metals in E-Waste recycling. *Minerals Engineering*, 191, Article 107969. <https://doi.org/10.1016/j.mineng.2022.107969>

---

This material is protected by copyright and other intellectual property rights, and duplication or sale of all or part of any of the repository collections is not permitted, except that material may be duplicated by you for your research use or educational purposes in electronic or print form. You must obtain permission for any other use. Electronic or print copies may not be offered, whether for sale or otherwise to anyone who is not an authorised user.



## Novel fluxing strategy of copper matte smelting and trace metals in E-Waste recycling

Min Chen<sup>a</sup>, Katri Avarmaa<sup>a,1</sup>, Pekka Taskinen<sup>a</sup>, Lassi Klemettinen<sup>a</sup>, Radoslaw Michallik<sup>b</sup>, Hugh O'Brien<sup>b</sup>, Ari Jokilaakso<sup>a,\*</sup>

<sup>a</sup> Department of Chemical and Metallurgical Engineering, School of Chemical Engineering, Aalto University, Kemistintie 1F, P.O. Box 16100, FI-00076 Aalto, Finland

<sup>b</sup> Geological Survey of Finland, Vuorimiehentie 2, 02150 Espoo, Finland

### ARTICLE INFO

#### Keywords:

Minor elements  
WEEE  
Sustainability  
Flash smelting  
Fluxing practice  
Circular economy

### ABSTRACT

The distribution behavior of trace metals between copper matte and spinel-saturated iron silicate slags was investigated at 1250 °C and  $p_{\text{SO}_2}$  of 0.25 atm at low silica concentrations. The experiments were conducted in magnetite ( $\text{Fe}_3\text{O}_4$ ) spinel crucibles in controlled  $\text{CO-CO}_2\text{-SO}_2\text{-Ar}$  gas mixtures using a high-temperature equilibrium-quenching technique. The concentrations of trace elements in matte, spinel, and slag were quantified by electron probe X-ray microanalysis and laser ablation-inductively coupled plasma-mass spectrometry. The trace metals (Ag, Ni, Co, and Sn) in all phases and their distribution coefficients were calculated as a function of matte grade. Results show that silver and nickel can be effectively recovered into matte, whereas cobalt and tin are predominantly deported into slag and gas phases, respectively. These results augment the fundamental thermodynamic data of trace metal distributions in copper smelting processes at low-silica fluxing practices.

### 1. Introduction

Secondary materials, including metallurgical wastes and waste electrical and electronic equipment (WEEE), are some of the fastest growing waste streams in the world (Ogunseitan et al. 2009; Tesfaye et al. 2017; Yang et al. 2017; Zhang and Xu, 2016). Urban mining and recycling of the valuable metals within these materials convey important economic and environmental benefits under the current situation of natural mineral resource depletion. Apart from the main metals contained in WEEE, the presence of (valuable) trace metals has increased the importance of WEEE recycling (Cui and Forssberg, 2003; Cesaro et al. 2018; Messmann et al. 2019).

The smelting technologies of base metals are efficient recycling methods for trace metals from secondary resources. Among these, the copper smelting routes are common on industrial scales (Brusselaers et al. 2006; Hagelüken, 2006a, 2006b; Lennartsson et al. 2018). Because of the thermodynamic properties of trace metals, they deport into different phases present (i.e., metal, matte, slag, gas, and spinel) in the smelting and refining processes. Therefore, the distribution equilibria of

trace metals in copper smelting processes are of great interest for improving the recoveries of trace metals from wastes. Additionally, hazardous heavy metals such as Pb, As, and Cd exist in copper smelting slags making it a source of emissions for surface water, soil, and groundwater (Shen and Forssberg, 2003; Zhang et al. 2021; Zhou et al. 2021). The utilization of copper smelting slags has been investigated broadly (Fan et al. 2018; Gorai and Jana, 2003; Košir et al. 2021; Lemougna et al. 2020; Shi et al. 2008; Wang and Erdenebold, 2020), but the utilization rate is very low. The disposal of the produced large quantities of copper slags requires large areas of land which may lead to human health challenges and loss of biodiversity due to the release of hazardous elements to the environment (Murari et al. 2015; Phiri et al. 2021, 2022). Additionally, these slag dump areas require continuous and long-term maintenance. Thus, by lowering the slag formation in the copper smelting processes, the slag amount in landfills and the subsequent release of hazardous elements to the environment can be effectively reduced, while improving the resource efficiency of valuable metals by reducing their amounts in the disposed slags. By decreasing the silica concentration in slags, the slag-to-matte/matte ratio of

\* Corresponding author at: P.O. Box 16100, FI-00076 Aalto, Finland.

E-mail addresses: [min.chen@aalto.fi](mailto:min.chen@aalto.fi) (M. Chen), [kavarmaa@swin.edu.au](mailto:kavarmaa@swin.edu.au) (K. Avarmaa), [pekka.taskinen@aalto.fi](mailto:pekka.taskinen@aalto.fi) (P. Taskinen), [lassi.klemettinen@aalto.fi](mailto:lassi.klemettinen@aalto.fi) (L. Klemettinen), [radoslaw.michallik@gtk.fi](mailto:radoslaw.michallik@gtk.fi) (R. Michallik), [hugh.obrien@gtk.fi](mailto:hugh.obrien@gtk.fi) (H. O'Brien), [ari.jokilaakso@aalto.fi](mailto:ari.jokilaakso@aalto.fi) (A. Jokilaakso).

<sup>1</sup> Current address: Department of Mechanical and Product Design Engineering, Swinburne University of Technology, John Str, Hawthorne, Melbourne, Victoria 3122, Australia.

<https://doi.org/10.1016/j.mineng.2022.107969>

Received 22 June 2022; Received in revised form 22 November 2022; Accepted 3 December 2022

Available online 12 December 2022

0892-6875/© 2022 The Author(s). Published by Elsevier Ltd. This is an open access article under the CC BY license (<http://creativecommons.org/licenses/by/4.0/>).

**Table 1**  
Materials used in the present study.

Material	Size and Purity	Supplier
Cu <sub>2</sub> S	–200 mesh, 99.5 wt%	Alfa Aesar
FeS	–100 mesh, 99.9 wt%	Alfa Aesar
Fe <sub>2</sub> O <sub>3</sub>	99.998 wt%	Alfa Aesar
SiO <sub>2</sub>	–40 mesh, 99.995 wt%	Alfa Aesar
Al <sub>2</sub> O <sub>3</sub>	99.99 wt%	Sigma-Aldrich
CaO	99.9 wt%	Sigma-Aldrich
Ag	–100 mesh, 99.95 wt%	Alfa Aesar
Ni	–120 mesh, 99.996 wt%	Alfa Aesar
Co	–1.6 μm, 99.8 wt%	Alfa Aesar
Sn	–325 mesh, 99.8 wt%	Alfa Aesar
CO	99.99 vol%	Woikoski Oy (Finland)
CO <sub>2</sub>	99.999 vol%	Woikoski Oy (Finland)
SO <sub>2</sub>	99.99 vol%	Woikoski Oy (Finland)
Ar	99.999 vol%	Woikoski Oy (Finland)
Iron foil	thickness 0.25 mm, 99.5 wt%	Sigma Aldrich & Merck

approximately 3 (w/w) in copper smelting and the resulting slag volume can be significantly decreased (Taskinen and Avarmaa, 2021).

The distributions of trace metals in copper smelting systems have not been investigated systematically at low silica concentrations, which are limited by magnetite ('spinel') saturation. Therefore, the aim of this study was to investigate the equilibrium distributions of selected trace metals (Ag, Ni, Co, and Sn) between copper matte, spinel, and iron silicate slags (FeO<sub>x</sub>-SiO<sub>2</sub>, FeO<sub>x</sub>-SiO<sub>2</sub>-Al<sub>2</sub>O<sub>3</sub>, and FeO<sub>x</sub>-SiO<sub>2</sub>-CaO) at 1250 °C and pSO<sub>2</sub> of 0.25 atm using magnetite crucibles that enabled the experimental conditions for low-silica slags. The present results help to deepen our understanding about the behaviors of trace metals in copper matte smelting processes at low silica concentrations and subsequently provide insights for improving the recoveries of metal values. The novel fluxing strategy proposed for copper smelting and trace metals recycling

from e-waste can effectively reduce the slag amount, minimize land-filling spaces, and lower the discharge of hazardous elements into the environment. Simultaneously, it improves resource efficiency by lowering the mass amount of valuable metals lost in slag. The slag-matte phase relations at the spinel primary phase field in the same experiments were reported in an earlier paper (Chen et al. 2022c).

**2. Experimental**

The starting materials used in this study are listed in Table 1. Sulfide powders of Cu<sub>2</sub>S and FeS were used to prepare the copper matte mixture. Approximately 1 wt% of each trace element (Ag, Ni, Co, and Sn) were introduced into the copper matte mixture in metallic powder form. The prepared copper matte mixture with an initial mass ratio of Cu<sub>2</sub>S/FeS = 70/30 was used for the ease of reaching different target matte grades within a short experimental time. The experiments in this study followed the molten slag-solid spinel phase boundary in the FeO<sub>x</sub>-SiO<sub>2</sub>, FeO<sub>x</sub>-SiO<sub>2</sub>-Al<sub>2</sub>O<sub>3</sub>, and FeO<sub>x</sub>-SiO<sub>2</sub>-CaO systems in equilibrium with controlled gas phase at 1250 °C. Based on the phase boundaries of the FeO<sub>x</sub>-SiO<sub>2</sub>, FeO<sub>x</sub>-SiO<sub>2</sub>-Al<sub>2</sub>O<sub>3</sub>, and FeO<sub>x</sub>-SiO<sub>2</sub>-CaO systems in equilibrium with a controlled gas atmosphere, predicted by MTDATA using its MTOX database (Davies et al. 2002; Gisby et al. 2017), slag mixtures with compositions of Fe<sub>2</sub>O<sub>3</sub>/SiO<sub>2</sub> = 80/20, Fe<sub>2</sub>O<sub>3</sub>/SiO<sub>2</sub>/Al<sub>2</sub>O<sub>3</sub> = 62/28/10, and Fe<sub>2</sub>O<sub>3</sub>/SiO<sub>2</sub>/CaO = 62/28/10 were employed to ensure that proper proportions of molten slag and solid spinel could be obtained for EPMA and LA-ICP-MS analyses. Phase diagrams of the FeO<sub>x</sub>-SiO<sub>2</sub> and FeO<sub>x</sub>-SiO<sub>2</sub>-Al<sub>2</sub>O<sub>3</sub> systems calculated by MTDATA have been reported previously (Chen et al. 2020a, 2021b). Fig. 1 shows the 1250 °C isothermal sections of the FeO<sub>x</sub>-SiO<sub>2</sub>-CaO phase diagram at pO<sub>2</sub> of 10<sup>-8</sup> and 10<sup>-7</sup> atm. The increase of oxygen partial pressure from 10<sup>-8</sup> to 10<sup>-7</sup> atm decreases the concentration of iron oxide in liquid slag while increasing

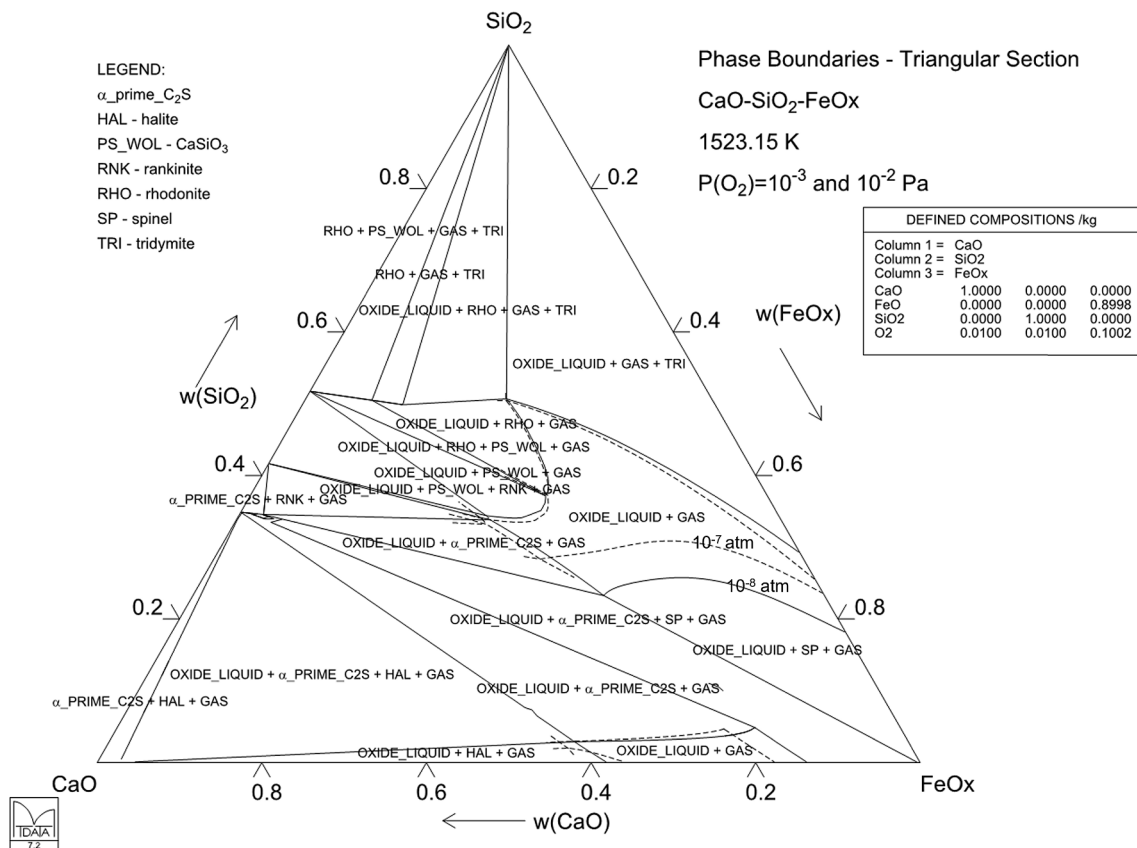


**Fig. 1.** Phase diagram of the FeO<sub>x</sub>-SiO<sub>2</sub>-CaO system at 1250 °C and pO<sub>2</sub> of 10<sup>-8</sup> and 10<sup>-7</sup> atm; solid line pO<sub>2</sub> = 10<sup>-8</sup> atm; dashed line pO<sub>2</sub> = 10<sup>-7</sup> atm (calculated using MTDATA and the MTOX database (Gisby et al. 2017)).

**Table 2**

The calculated gas flowrates at  $p_{\text{SO}_2}$  of 0.25 atm for different target  $p_{\text{O}_2}$  and  $p_{\text{S}_2}$  at 1250 °C.

$\text{Log}_{10}[p_{\text{O}_2}, \text{atm}]$	$\text{Log}_{10}[p_{\text{S}_2}, \text{atm}]$	Gas flow rates ( $\text{mL}\cdot\text{min}^{-1}$ )			
		$\text{SO}_2$	$\text{CO}$	$\text{CO}_2$	$\text{Ar}$
-7.50	-3.41	100.0	4.8	98.6	200.0
-7.62	-3.17	100.0	5.9	96.8	200.0
-7.75	-2.91	100.0	7.5	94.1	200.0
-7.84	-2.73	100.0	9.0	91.0	200.0
-7.90	-2.62	100.0	10.5	91.5	200.0

silica concentration at the spinel saturation boundary.

In each experiment, 0.2 g of copper matte mixture and the same amount of slag mixture were pressed into a cylindrical pellet. The spinel ( $\text{Fe}_3\text{O}_4$ ) crucible used for holding the sample pellet was prepared by oxidizing a folded iron foil at 1200 °C and  $p_{\text{O}_2}$  of  $10^{-8}$  atm for 4 h. The use of spinel crucibles ensured spinel saturation in slags equilibrated with copper matte. The calculated gas flow rates of  $\text{CO}$ ,  $\text{CO}_2$ ,  $\text{SO}_2$ , and  $\text{Ar}$  for different target  $p_{\text{O}_2}$  and  $p_{\text{S}_2}$  were calculated with MTDATA using its SGTE database (Davies et al. 2002; Gisby et al. 2017), shown in Table 2.

In general, the experiments in the present study followed the route of sample preparation, high-temperature isothermal equilibration of samples in spinel crucibles, ice-water quenching, and direct phase composition analyses. A vertical tube furnace (Lenton PTF) heated by SiC heating elements with a three-zone temperature control technique was used for the equilibration experiments. An S-type Pt/Pt-10 %Rh thermocouple (Johnson-Matthey Noble Metals, UK) in an alumina sheath was placed next to the sample in the reaction tube for monitoring the sample temperature, as shown in Fig. 2. Preliminary experiments were carried out by equilibrating copper matte and  $\text{FeO}_x\text{-SiO}_2$  slag at 1250 °C,  $p_{\text{SO}_2} = 0.25$  atm,  $p_{\text{O}_2} = 10^{-7.75}$  atm, and  $p_{\text{S}_2} = 10^{-2.91}$  atm for testing different equilibration times ranging from 2 to 6 h. The compositions of the matte and slag phases were found to stay constant after 4 h (Chen et al. 2022c). Therefore, all samples were annealed at the given conditions for 4 h in this study. Detailed experimental methodology can be

found in the literature (Avarmaa et al. 2015, 2016; Chen et al. 2020a, 2020b, 2020c, 2021b).

The equilibrated samples were quenched into ice-water mixtures to retain the high-temperature equilibrium phase assemblages at room temperature. The quenched condensed phases were mounted in epoxy, polished, and carbon coated using a carbon evaporator device (JEOL IB-29510VET). The major elemental compositions and microstructures of samples were pre-examined using a scanning electron microscope (SEM, Tescan MIRA 3, Brno, Czech Republic) equipped with an UltraDry Silicon Drift Energy Dispersive X-ray Spectrometer (EDS, Thermo Fisher Scientific, Waltham, MA, USA). A Cameca SX100 electron probe microanalyzer (EPMA, Cameca SAS, Genevilliers, France) at the Geological Survey of Finland (GTK) was used to measure the concentrations of major elements and trace metals in all phases using wave dispersive spectroscopy (WDS) analysis. A defocused beam with 20  $\mu\text{m}$  diameter was used for the matte and slag phases and 10  $\mu\text{m}$  diameter beam for the spinel phase. A new three-spot analytical method was adopted for the matte and slag phases, shown in detail in our previous publications (Chen et al. 2021b, 2022b). The EPMA analyses were carried out with an accelerating voltage of 20 kV and a beam current of 60nA. Analytical results were corrected using the PAP on-line correction

**Table 3**

Standards used for EPMA analyses in the present study.

Element	X-ray line	Standard
O	$\text{K}\alpha$	Obsidian
Si	$\text{K}\alpha$	Quartz
Co	$\text{K}\alpha$	Cobaltite
Ni	$\text{K}\alpha$	Metallic nickel
Cu	$\text{K}\alpha$	Metallic copper
Ag	$\text{L}\alpha$	Metallic silver
Al	$\text{K}\alpha$	Almandine
Ca	$\text{K}\alpha$	Diopside
Fe	$\text{K}\alpha$	Chalcopyrite
Sn	$\text{L}\alpha$	Metallic tin
S	$\text{K}\alpha$	Chalcopyrite

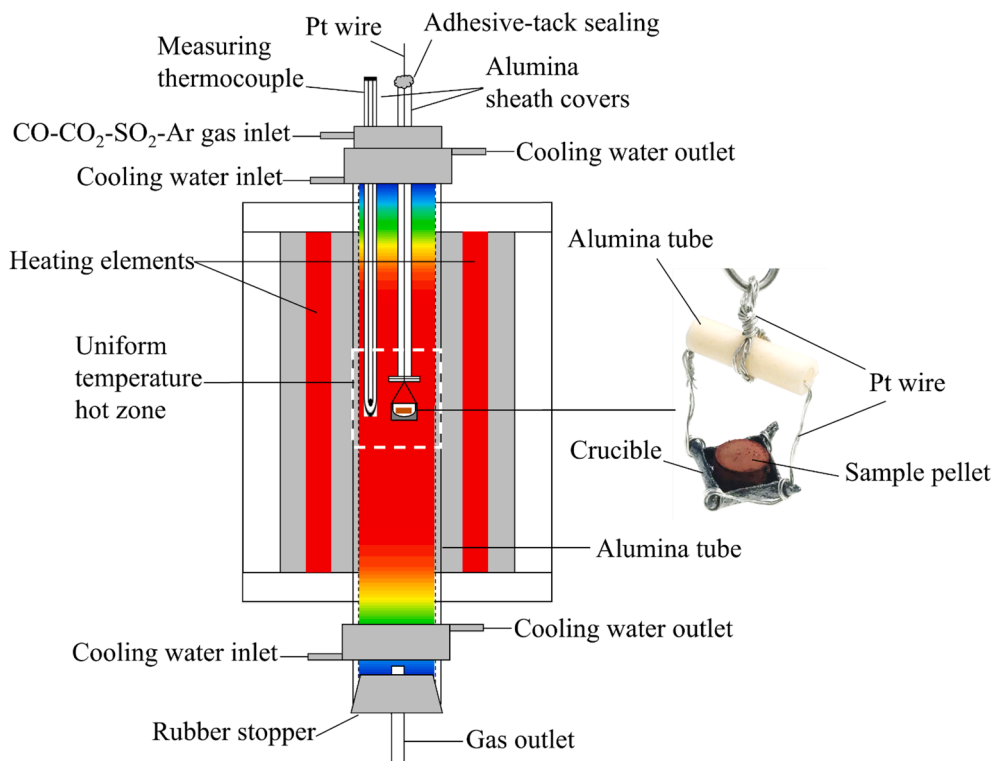


Fig. 2. Schematic of the equilibrium furnace and the sample holding arrangement.

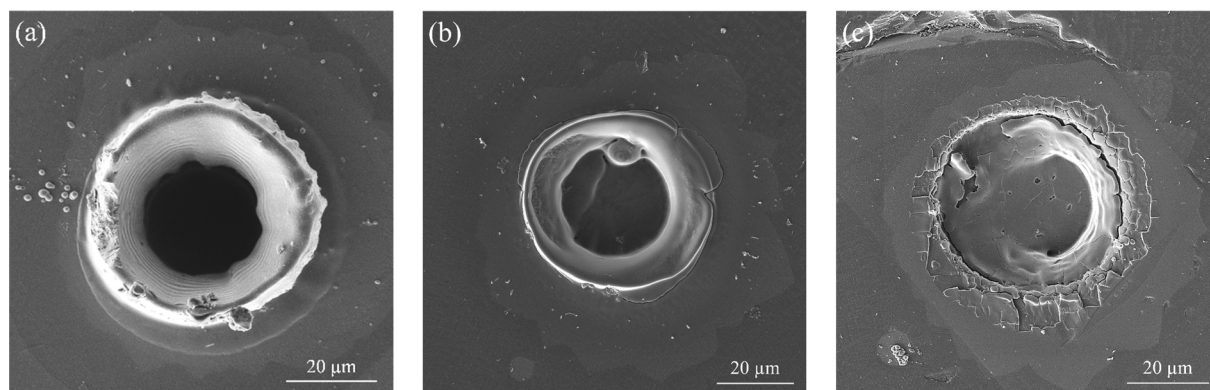


Fig. 3. Laser pits in different phases; (a) matte; (b) slag; (c) spinel.

Table 4  
Elemental detection limits of EPMA and LA-ICP-MS/ppmw.

Technique	Phase	O	Si	Co	Ni	Cu	Ag	Al	Ca	Fe	Sn	S
EPMA	Matte	766	157	144	245	334	389	179	78	126	292	127
	Slag	1072	142	200	230	216	327	143	68	147	252	102
	Spinel	988	147	225	187	220	263	162	69	170	266	107
LA-ICP-MS		<sup>29</sup> Si	<sup>57</sup> Fe	<sup>107</sup> Ag	<sup>60</sup> Ni	<sup>59</sup> Co	<sup>120</sup> Sn					
	Matte	7.620	1.750	0.009	0.180	0.014	0.033					
	Slag	10.250	1.870	0.005	0.170	0.013	0.039					
	Spinel	11.130	2.070	0.007	0.190	0.015	0.043					

program (Pouchou and Pichoir, 1986). Natural minerals and synthetic metals were used as standards for EPMA analyses, as shown in Table 3.

The concentrations of some trace metals in matte, slag, and spinel were lower than the detection limits of EPMA. Therefore, laser ablation-inductively coupled plasma-mass spectrometry (LA-ICP-MS) housed at the Geological Survey of Finland (GTK) was also employed to determine the concentrations of all trace metals in all phases. The equipment used combined a Nu AttoM SC-ICP-MS (Nu Instruments ltd, Wrexham, UK) and a Photon Machines Analyte Excite 193 nm ArF laser ablation equipment (Photon Machines, San Diego, USA). The laser was set to a pulse frequency of 10 Hz and a pulse energy of 5 mJ at 30 % attenuation, leading to an energy flux of 2.17 J/cm<sup>2</sup> on the sample surface with a 40 μm spot size. Fig. 3 shows the laser pits produced in matte, slag, and spinel phases.

The analyses were initiated with a 20 s baseline measurement followed by switching on the laser for 35 s (350 laser pulses) for signal acquisition in all phases. The time-resolved analysis (TRA) signals were

collected using the fast-scanning mode at low resolution ( $M/\Delta M = 300$ ). For the slag and spinel phases, GSE-1G glass and <sup>57</sup>Fe were used as the external and internal standard, respectively. Reference materials GSD-1G and BHVO-2G were analyzed as unknowns for monitoring the data accuracy. For the matte phase, FeS-1 was employed as the external standard and FeS-6 was used as a reference material for quality control. Isotopes of <sup>107</sup>Ag for silver, <sup>60</sup>Ni for nickel, <sup>59</sup>Co for cobalt, and <sup>120</sup>Sn for tin were used for calculating the concentrations of trace metals. The time-resolved analysis signal processing was performed using the Glitter software (Van Achterbergh, 2001). Table 4 presents the elemental detection limits of EPMA and LA-ICP-MS estimated in these measurements.

The obtained TRA signals generally showed very homogeneous dissolution of the trace elements in the analyzed volumes of the matte phase, as shown in Fig. 4(a), but some of the Ag signals showed evidence of heterogeneous areas. Homogeneous dissolution was also generally observed in the slag phase, however, the elemental concentrations and

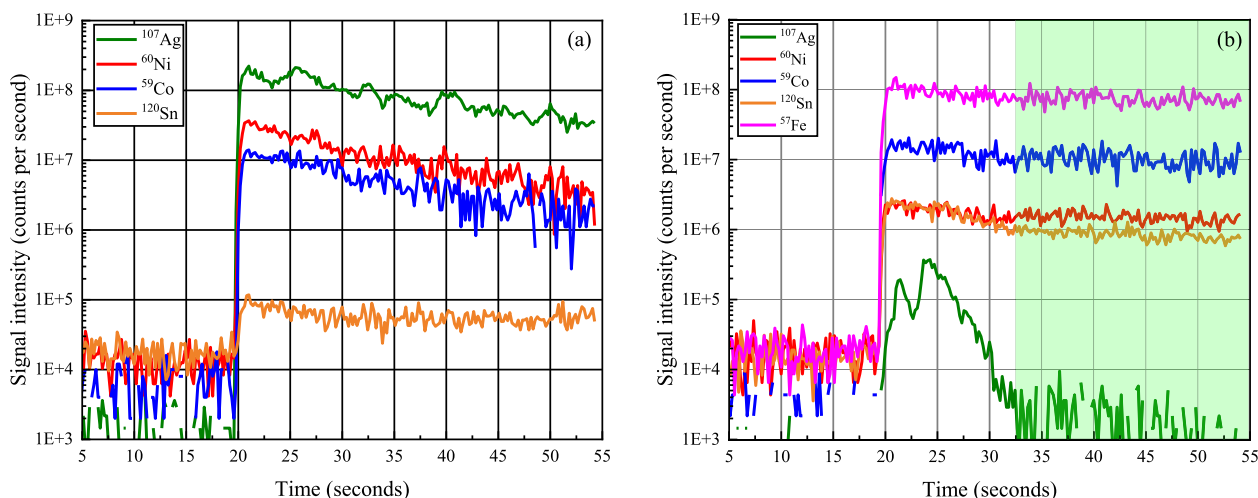


Fig. 4. Examples of TRA signals in matte (a) and spinel (b) as a function of analysis time.

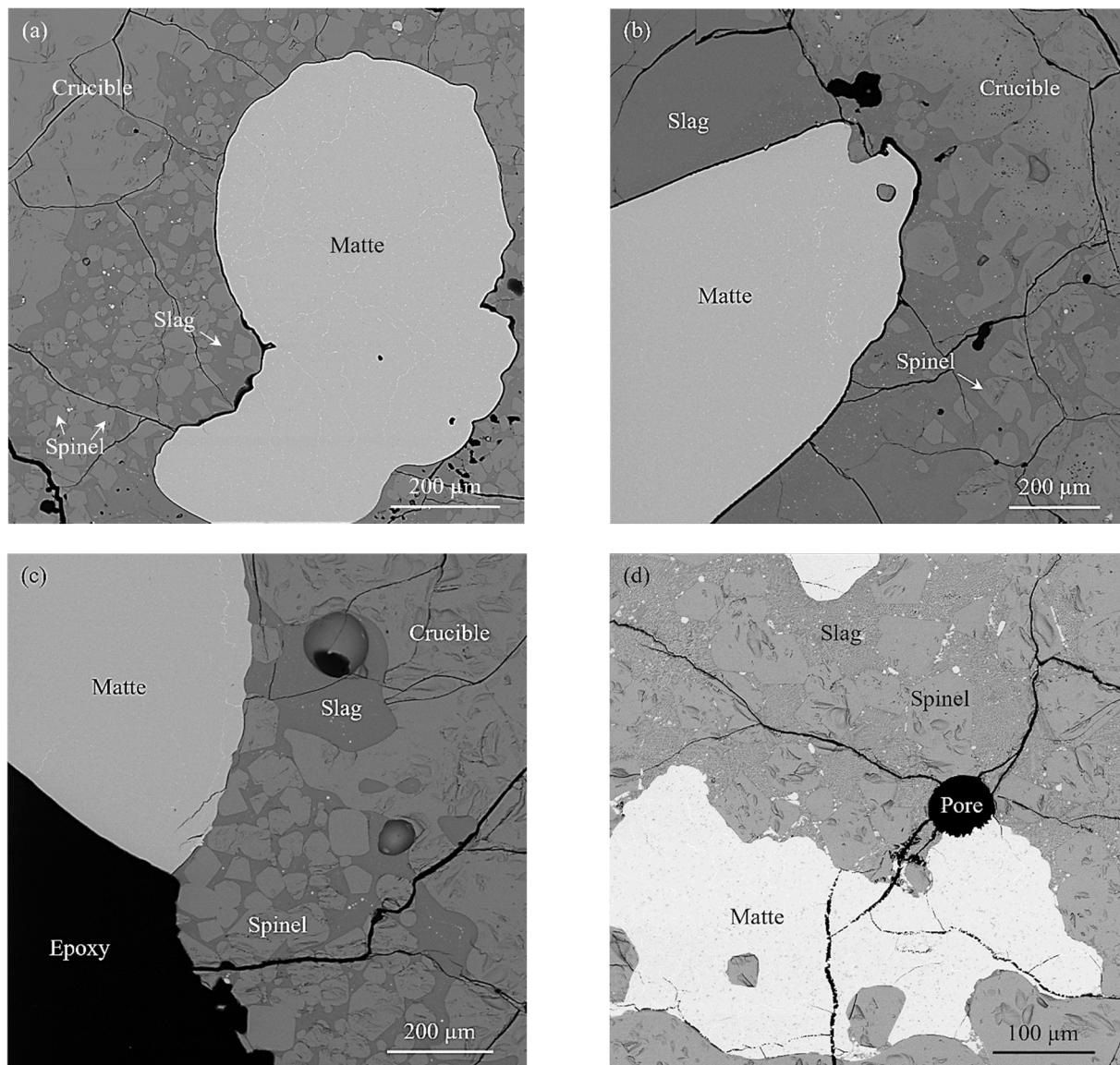


Fig. 5. Typical microstructures of the matte phase in equilibrium with spinel and different slags; (a) and (d)  $\text{FeO}_x\text{-SiO}_2$ ; (b)  $\text{FeO}_x\text{-SiO}_2\text{-Al}_2\text{O}_3$ ; and (c)  $\text{FeO}_x\text{-SiO}_2\text{-CaO}$ .

homogeneity varied in the magnetite spinels, as shown in Fig. 4(b). The continuity of Fe signals in Fig. 4(b) indicates that the laser was burning through the spinel grain during the entire analysis. The Ag signals in spinel showed large peaks in many instances, corresponding to Ag-containing nano- or micro inclusions. Signal areas free of these inclusions were used for concentration quantifications by limiting the great signal variations out from the analyses, as shown in Fig. 4(b) with the green rectangle. The Sn signals generally showed homogeneous dissolution, however, the concentration variations were much greater from one spinel crystal to another when compared to the deviations of the other minor metals. The dissolution of Ni and Co was the most homogeneous in the spinels analyzed out of the four trace metals investigated in the present study.

### 3. Results and discussion

Fig. 5 represents typical microstructures of the matte-slag-spinel-gas equilibrium systems obtained at 1250 °C,  $p\text{O}_2$  of  $10^{-7.50}$  atm, and  $p\text{S}_2$  of  $10^{-3.41}$  atm. Copper and trace metals segregations, most likely formed during quenching, were observed in the matte phase. That is typical to sulfide mattes which are extremely difficult to quench into glassy form.

Some physically entrained copper matte droplets were observed in the slag, and they were aggregated to the edges of the spinel crystals (Bellemans et al. 2018a, 2018b; De Wilde et al. 2016a, 2016b, 2017), as shown in Fig. 5(d). The concentrations of trace metals in matte, slag, and spinel with standard deviations ( $\pm 1\sigma$ ) are shown in Table 5.

#### 3.1. Concentrations of trace metals in matte

Fig. 6 presents the concentrations of trace metals in matte as a function of matte grade, Ag and Ni measured by EPMA, whereas Co and Sn by LA-ICP-MS. Fig. 6(a) shows that the concentration of silver dissolved in all mattes equilibrated with spinel-saturated iron silicate slags kept almost constant over the entire matte grade range studied, fluctuating around 1 wt%. Evidence of areas with heterogeneous dissolution of Ag was found from some of the time-resolved signals from the mass spectrometer in LA-ICP-MS analyses. Additionally, silver begins to volatilize in the experimental conditions, possibly resulting in concentration gradients in the matte phase. Due to these two reasons, the standard deviations of silver are somewhat higher than those of the other trace elements. The present results for silver obtained at 1250 °C and  $p\text{SO}_2$  of 0.25 atm are close to the data presented by Avarmaa et al.

Table 5

Concentrations of trace metals in matte, slag, and spinel at 1250 °C and  $p\text{SO}_2$  of 0.25 atm measured by EPMA and LA-ICP-MS.

Type of slag	Code	Average concentration in matte					Average concentration in slag by LA-ICP-MS				Average concentration in spinel by LA-ICP-MS				
		*Cu/wt %	**Ag/wt%	**Ni/wt%	*Co/wt%	*Sn/ppmw	Ag/ppmw	Ni/wt %	Co/wt %	Sn/ppmw	Ag/ppmw	Ni/wt %	Co/wt %	Sn/ppmw	
FeO <sub>x</sub> -SiO <sub>2</sub>	CSP-14	75.29 ± 0.41	1.01 ± 0.31	0.64 ± 0.11	0.06 ± 0.00	2.72 ± 0.25	26.27 ± 4.32	0.11 ± 0.01	0.28 ± 0.01	44.13 ± 6.56	0.09 ± 0.09	0.32 ± 0.04	0.26 ± 0.01	190.24 ± 146.10	
	CSP-39	75.04 ± 0.33	1.14 ± 0.36	0.70 ± 0.36	0.07 ± 0.00	4.35 ± 1.65	18.12 ± 0.85	0.07 ± 0.00	0.28 ± 0.01	40.49 ± 4.12	0.10 ± 0.11	0.16 ± 0.00	0.25 ± 0.01	118.31 ± 134.97	
	CSP-15	72.80 ± 0.42	0.93 ± 0.28	0.84 ± 0.28	0.09 ± 0.00	4.64 ± 0.35	11.17 ± 2.69	0.06 ± 0.01	0.21 ± 0.01	15.66 ± 2.23	0.04 ± 0.03	0.13 ± 0.03	0.18 ± 0.03	42.11 ± 36.94	
	CSP-40	73.08 ± 0.40	0.95 ± 0.39	0.80 ± 0.39	0.10 ± 0.01	5.00 ± 0.67	18.45 ± 8.08	0.08 ± 0.04	0.26 ± 0.02	28.31 ± 9.04	0.12 ± 0.20	0.19 ± 0.06	0.22 ± 0.04	76.49 ± 107.65	
	CSP-16	70.08 ± 0.31	0.70 ± 0.31	0.81 ± 0.31	0.14 ± 0.03	3.39 ± 0.61	22.08 ± 5.87	0.08 ± 0.01	0.26 ± 0.02	9.86 ± 1.54	0.01 ± 0.00	0.15 ± 0.01	0.21 ± 0.01	193.25 ± 118.56	
	CSP-41	69.99 ± 0.77	1.05 ± 0.51	0.79 ± 0.51	0.13 ± 0.01	4.79 ± 0.28	18.21 ± 11.70	0.07 ± 0.01	0.23 ± 0.01	22.28 ± 3.86	0.04 ± 0.02	0.19 ± 0.01	0.20 ± 0.01	126.74 ± 139.93	
	CSP-17	65.57 ± 0.25	0.91 ± 0.25	0.73 ± 0.25	0.18 ± 0.01	4.21 ± 0.34	40.34 ± 6.65	0.07 ± 0.00	0.22 ± 0.01	11.13 ± 2.13	0.03 ± 0.03	0.13 ± 0.01	0.17 ± 0.02	43.40 ± 38.50	
	CSP-42	65.56 ± 0.56	0.88 ± 0.38	0.81 ± 0.38	0.17 ± 0.01	6.02 ± 0.42	17.11 ± 6.35	0.06 ± 0.01	0.23 ± 0.01	17.20 ± 1.79	0.06 ± 0.07	0.11 ± 0.00	0.19 ± 0.01	48.98 ± 81.06	
	CSP-18	60.81 ± 0.64	0.91 ± 0.11	0.73 ± 0.14	0.21 ± 0.01	4.65 ± 0.60	80.35 ± 19.05	0.08 ± 0.00	0.20 ± 0.01	8.34 ± 0.89	0.02 ± 0.00	0.10 ± 0.01	0.17 ± 0.03	51.65 ± 68.17	
	CSP-43	61.26 ± 0.73	0.88 ± 0.22	0.70 ± 0.22	0.19 ± 0.00	5.32 ± 1.21	35.96 ± 8.16	0.08 ± 0.01	0.20 ± 0.01	11.29 ± 1.19	0.03 ± 0.02	0.10 ± 0.00	0.15 ± 0.00	25.92 ± 30.50	
	FeO <sub>x</sub> -SiO <sub>2</sub> -Al <sub>2</sub> O <sub>3</sub>	CSP-19	75.65 ± 0.50	0.89 ± 0.49	0.49 ± 0.16	0.06 ± 0.00	5.16 ± 0.86	42.43 ± 8.11	0.08 ± 0.01	0.26 ± 0.01	27.49 ± 1.00	0.23 ± 0.23	0.18 ± 0.05	0.24 ± 0.05	57.89 ± 80.70
		CSP-20	75.23 ± 0.40	0.94 ± 0.37	0.50 ± 0.13	0.04 ± 0.00	8.06 ± 1.08	71.80 ± 8.30	0.12 ± 0.00	0.19 ± 0.00	33.06 ± 1.55	0.11 ± 0.09	0.24 ± 0.04	0.16 ± 0.01	73.07 ± 100.42
		CSP-21	73.57 ± 0.71	0.94 ± 0.43	0.73 ± 0.14	0.08 ± 0.01	5.23 ± 0.56	12.99 ± 0.26	0.04 ± 0.00	0.16 ± 0.00	23.51 ± 0.80	0.02 ± 0.01	0.20 ± 0.07	0.20 ± 0.04	62.21 ± 113.92
		CSP-22	73.15 ± 0.29	1.12 ± 0.31	0.80 ± 0.08	0.08 ± 0.00	2.59 ± 0.21	26.30 ± 6.07	0.08 ± 0.01	0.24 ± 0.01	9.40 ± 1.82	0.04 ± 0.04	0.11 ± 0.03	0.18 ± 0.03	16.52 ± 18.20
		CSP-23	70.38 ± 0.26	0.85 ± 0.33	0.73 ± 0.04	0.10 ± 0.00	4.72 ± 0.44	68.76 ± 11.95	0.09 ± 0.01	0.18 ± 0.00	10.80 ± 0.39	0.06 ± 0.07	0.16 ± 0.06	0.17 ± 0.04	52.10 ± 61.30
		CSP-24	71.03 ± 0.60	0.95 ± 0.44	0.63 ± 0.06	0.10 ± 0.01	2.88 ± 0.26	13.71 ± 2.68	0.07 ± 0.00	0.19 ± 0.01	5.43 ± 0.27	0.08 ± 0.10	0.18 ± 0.02	0.17 ± 0.02	78.03 ± 130.88
		CSP-25	66.79 ± 0.52	1.01 ± 0.45	0.83 ± 0.09	0.15 ± 0.01	5.51 ± 0.29	22.46 ± 6.25	0.06 ± 0.00	0.20 ± 0.01	14.06 ± 2.29	0.08 ± 0.11	0.11 ± 0.02	0.16 ± 0.02	49.86 ± 56.07
		CSP-26	67.25 ± 0.31	1.03 ± 0.32	0.79 ± 0.13	0.14 ± 0.00	3.87 ± 0.36	21.25 ± 9.21	0.04 ± 0.00	0.12 ± 0.01	9.38 ± 2.83	0.06 ± 0.07	0.10 ± 0.02	0.13 ± 0.02	18.75 ± 22.79
CSP-27		62.92 ± 0.71	0.97 ± 0.24	0.86 ± 0.07	0.21 ± 0.01	6.50 ± 0.73	49.63 ± 16.72	0.07 ± 0.01	0.20 ± 0.01	9.84 ± 0.99	0.19 ± 0.14	0.12 ± 0.01	0.18 ± 0.02	60.56 ± 65.31	
CSP-28		63.02 ± 0.84	0.90 ± 0.18	0.72 ± 0.06	0.16 ± 0.01	4.00 ± 0.34	19.75 ± 6.12	0.04 ± 0.00	0.17 ± 0.01	11.23 ± 1.09	0.07 ± 0.04	0.08 ± 0.00	0.15 ± 0.01	33.56 ± 33.68	
FeO <sub>x</sub> -SiO <sub>2</sub> -CaO		CSP-29	74.75 ± 0.39	1.20 ± 0.30	0.70 ± 0.14	0.07 ± 0.00	3.14 ± 0.85	50.88 ± 5.75	0.15 ± 0.00	0.29 ± 0.00	16.27 ± 0.18	0.07 ± 0.05	0.26 ± 0.06	0.25 ± 0.02	11.30 ± 3.48
		CSP-30	74.76 ± 0.32	1.17 ± 0.33	0.68 ± 0.08	0.07 ± 0.00	5.17 ± 0.55	52.32 ± 7.58	0.14 ± 0.01	0.27 ± 0.01	15.83 ± 0.86	0.04 ± 0.06	0.28 ± 0.06	0.26 ± 0.02	73.68 ± 75.08
		CSP-31	72.90 ± 0.39	0.99 ± 0.30	0.71 ± 0.08	0.10 ± 0.01	5.93 ± 0.70	9.74 ± 2.39	0.08 ± 0.01	0.24 ± 0.01	14.04 ± 1.51	0.03 ± 0.02	0.18 ± 0.05	0.22 ± 0.03	31.94 ± 26.70
		CSP-32	72.81 ± 0.29	1.05 ± 0.18	0.82 ± 0.04	0.08 ± 0.00	6.54 ± 0.94	13.09 ± 5.28	0.09 ± 0.02	0.20 ± 0.02	14.57 ± 2.90	0.02 ± 0.01	0.16 ± 0.01	0.18 ± 0.02	8.90 ± 5.00
		CSP-33	69.18 ± 0.63	0.98 ± 0.34	0.80 ± 0.05	0.15 ± 0.01	6.79 ± 0.60	24.19 ± 3.84	0.08 ± 0.00	0.22 ± 0.01	10.26 ± 0.83	0.07 ± 0.05	0.20 ± 0.03	0.23 ± 0.03	15.48 ± 4.33
		CSP-34	69.57 ± 0.29	0.86 ± 0.29	0.78 ± 0.04	0.12 ± 0.00	8.14 ± 0.79	48.28 ± 5.08	0.07 ± 0.02	0.18 ± 0.02	11.92 ± 0.90	0.02 ± 0.01	0.13 ± 0.01	0.21 ± 0.01	33.84 ± 31.78
		CSP-35	65.03 ± 0.38	0.91 ± 0.22	0.84 ± 0.04	0.19 ± 0.00	8.26 ± 0.59	22.55 ± 8.81	0.06 ± 0.01	0.19 ± 0.01	12.80 ± 1.61	0.04 ± 0.02	0.12 ± 0.01	0.18 ± 0.00	9.70 ± 5.43
		CSP-36	64.63 ± 0.91	0.97 ± 0.22	0.75 ± 0.04	0.17 ± 0.01	8.12 ± 0.63	43.41 ± 16.67	0.05 ± 0.01	0.17 ± 0.01	9.17 ± 1.48	0.03 ± 0.02	0.08 ± 0.01	0.14 ± 0.01	15.58 ± 25.91
	CSP-37	61.02 ± 1.05	0.81 ± 0.24	0.67 ± 0.06	0.19 ± 0.01	7.31 ± 0.81	55.29 ± 9.45	0.06 ± 0.01	0.15 ± 0.01	9.74 ± 0.57	0.02 ± 0.01	0.10 ± 0.00	0.14 ± 0.00	7.81 ± 2.86	
	CSP-38	60.50 ± 1.22	0.91 ± 0.23	0.78 ± 0.07	0.19 ± 0.01	6.70 ± 0.66	95.81 ± 19.90	0.07 ± 0.01	0.17 ± 0.01	8.94 ± 0.69	0.07 ± 0.09	0.10 ± 0.00	0.15 ± 0.00	58.90 ± 58.94	

\* LA-ICP-MS measurement.

\*\* EPMA measurement.

(2016). The comparison of the present results obtained at spinel saturation in slags with previous data (Chen et al. 2020a, 2021a) determined at silica saturation indicates that the type of slag saturation and  $p\text{SO}_2$  had little impact on the concentration of silver in matte. Additions of alumina and lime were shown to have no impact on the concentrations of silver in matte, similar as our previous observations at silica

saturation (Chen et al. 2020a, 2021a).

The nickel concentration in matte, as shown in Fig. 6(b), stayed almost constant at 0.8 wt% over the matte grade range from 60 to 70 wt % Cu, after which it slightly decreased with increasing matte grade. Fig. 6(c) indicates that the cobalt concentration in matte had a linear decreasing trend from approximately 0.2 to 0.05 wt% over the entire

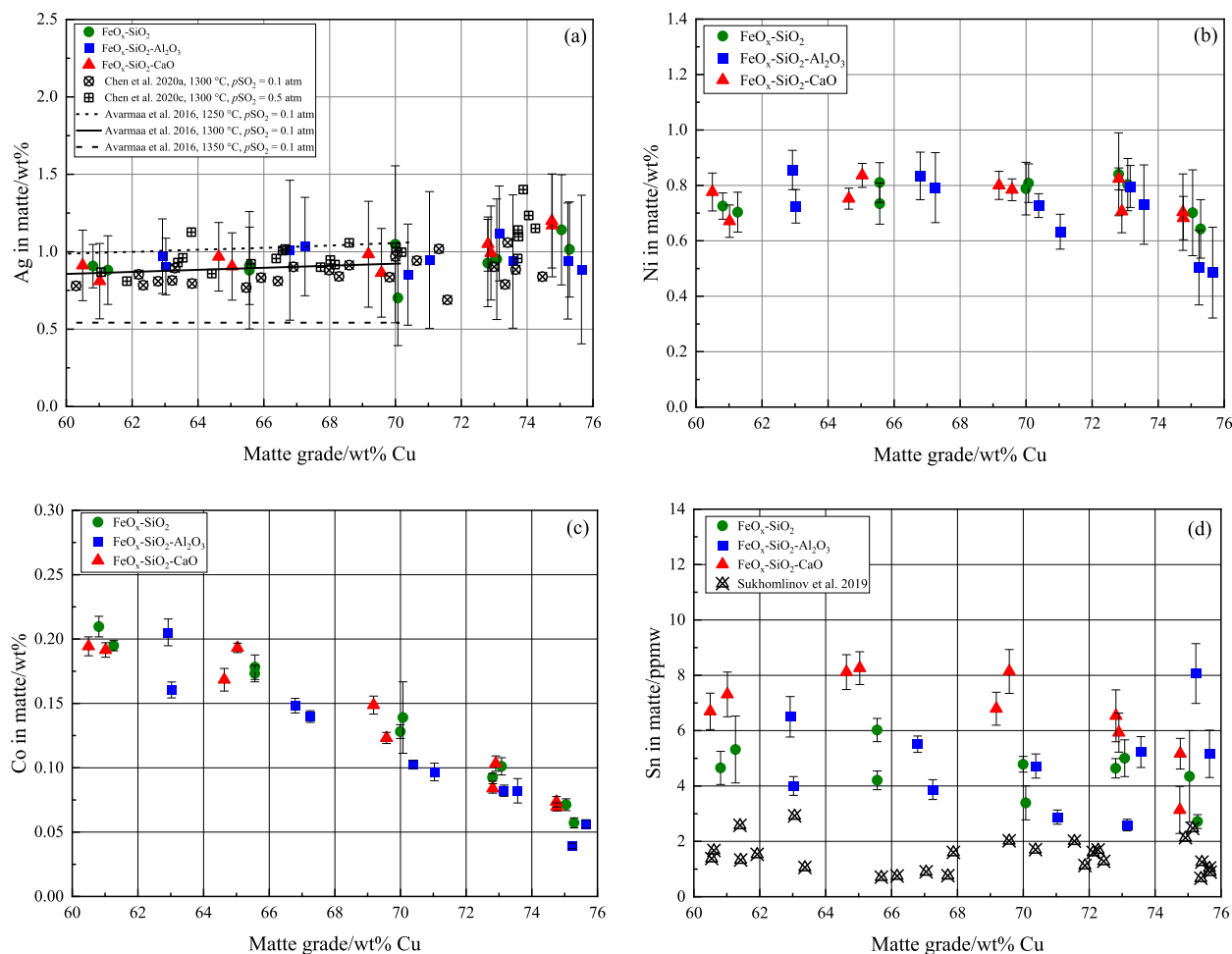


**Fig. 6.** Concentrations of trace elements in matte vs matte grade at 1250 °C and  $p\text{SO}_2$  of 0.25 atm: (a) silver by EPMA; (b) nickel by EPMA; (c) cobalt by LA-ICP-MS; and (d) tin by LA-ICP-MS.

matte grade range investigated, independent of slag modifiers.

Tin exhibited the lowest concentration in matte, ranging from 2 to 8 ppm. At spinel saturation, CaO addition in iron silicate slag led to a small increase in tin concentrations at a given matte grade, whereas the effect of  $\text{Al}_2\text{O}_3$  was not evident. The data by Sukhomlinov et al. (2019) for tin in matte obtained from silica saturated iron silicate slags are even lower than the present results. They also found that the concentration of tin in matte was not affected by slag modifiers  $\text{Al}_2\text{O}_3$  and CaO.

### 3.2. Concentrations of trace metals in slag

The concentrations of trace metals measured by LA-ICP-MS in spinel-saturated iron silicate slags with the experimental concentration variability ( $\pm 1\sigma$ ) are shown in Fig. 7. Fig. 7(a) indicates that the silver concentration in all spinel-saturated slags decreased with increasing matte grade from 60 to approximately 70 wt% Cu, after which it started to display an increasing trend at the higher matte grade range. The effects of alumina and lime on the concentration of silver in the spinel-saturated slag were not evident within the uncertainty of the present results. However, lime was found to have a decreasing impact on silver concentration in silica-saturated slags in our previous studies (Chen et al. 2020a, 2021a). Avarmaa et al. (2015) observed that higher temperature decreased the loss of silver in the silica-saturated iron silicate slags but increased its volatilization into the gas stream.

Fig. 7(b) shows that nickel concentration in all spinel-saturated slags in the present study kept nearly constant at approximately 0.06 wt% when the matte grade varied from 60 to 70 wt% Cu and tended to

increase at higher matte grades. The dissolution of nickel in the present spinel-saturated slags was not affected strongly by the slag modifiers. The concentration of cobalt in all slags displayed slightly increasing trends with increasing matte grade in the present study, as shown in Fig. 7(c). Additions of alumina and lime into spinel-saturated iron silicate slags slightly decreased the concentration of cobalt in slags.

Fig. 7(d) shows that the concentration of tin in  $\text{FeO}_x\text{-SiO}_2$  slag increased from approximately 10 to 40 ppm over the increasing matte grade range investigated. However, the concentration of tin in  $\text{FeO}_x\text{-SiO}_2\text{-Al}_2\text{O}_3$  and  $\text{FeO}_x\text{-SiO}_2\text{-CaO}$  slags kept almost constant at 10 ppm over the matte grade range from 60 to 70 wt% Cu, after which it increased with the increasing matte grade. Alumina and lime had decreasing impact on the tin concentration in slag, especially at matte grades higher than 70 wt% Cu. It should be noted that most tin vaporized during the experiments. The tin concentrations in silica-saturated iron silicate slags determined by Sukhomlinov et al. (2019) were lower than 10 ppm and the effects of alumina and lime were not evident in their study.

### 3.3. Concentrations of trace metals in iron spinel

The magnetite spinel is a common phase formed in the copper smelter, e.g., in the freeze lining or when the feed materials react in the reaction shaft of the flash smelting furnace (Jansson et al. 2015; Taskinen et al. 2011, 2013; Taskinen and Jokilaakso, 2021). The concentrations of trace metals in spinel in the present study were measured by LA-ICP-MS to get a big picture of their distributions, as shown in Fig. 8.

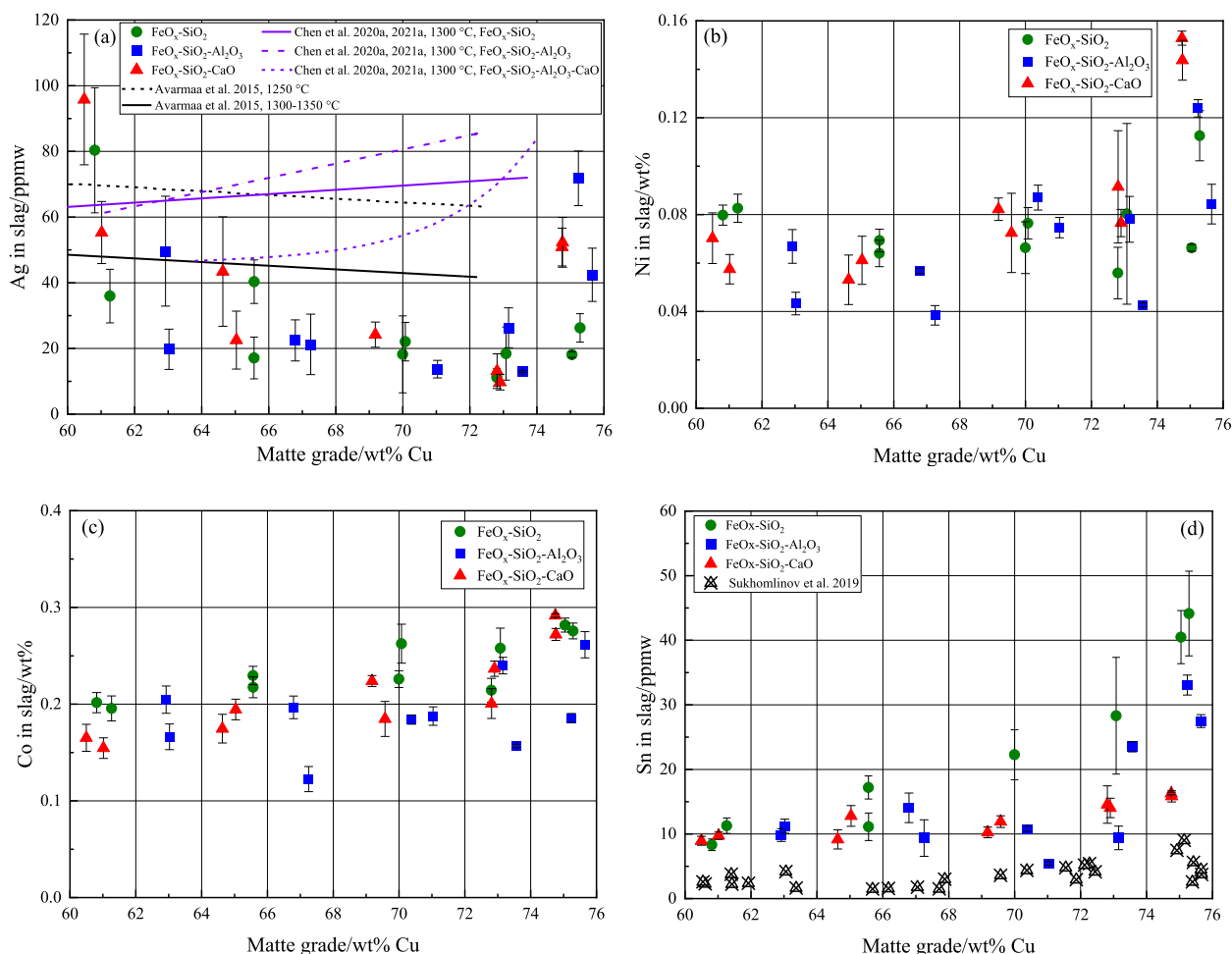


Fig. 7. Concentrations of trace metals in spinel-saturated iron silicate slags measured by LA-ICP-MS: (a) silver; (b) nickel; (c) cobalt; and (d) tin.

Silver exhibited the lowest dissolution in spinel (<1 ppm) when compared with the other trace metals investigated in the present study, similar to our previous observations (Chen et al. 2021b) in the Fe-spinel saturated copper-slag system at 1200–1300 °C. The concentrations of nickel and cobalt in the spinel had similar increasing trends with increasing matte grade, independent of the slag modifiers used. The concentration of cobalt in spinel was around 0.05 wt% higher than that of nickel when the matte grade was lower than 70 wt% Cu. The concentration of tin in spinel varied between zero and approximately 300 ppm without a clear trend and with a large standard deviation when compared to the other minor metals in the system.

### 3.4. Distribution coefficients between matte and slag

The logarithmic distribution coefficients of trace metals between copper matte and slag,  $\text{Log}_{10}L^{M/S}[\text{Me}]$ , were calculated using the following equation [1]:

$$\text{Log}_{10}L^{M/S}[\text{Me}] = \text{Log}_{10}([\text{wt}^{\%}\text{Me}]_{\text{inmatte}}/(\text{wt}^{\%}\text{Me})_{\text{in slag}}) \quad (1)$$

where [wt% Me] and (wt% Me) represent the average concentrations of trace metals in matte and slag, respectively. The calculated logarithmic distribution coefficients of all trace metals investigated in the present study as a function of matte grade are shown in Fig. 9. The present experimental results were compared with the selected data from the literature at different saturations and temperatures (Avarmaa et al. 2015; Chen et al. 2021a; Chen et al. 2022a; Hidayat et al. 2016; Roghani et al. 1997, 2000; Shishin et al. 2019; Sukhomlinov et al. 2019; Yazawa

et al. 1983). Most literature data were equilibrium results from laboratory experiments with silica saturation except the results by Chen et al. (2022a). They investigated Fe-spinel saturated industrial samples from copper matte converting conditions of the Peirce-Smith process which means their samples may not have reached true equilibrium and included trace levels of many elements. Hidayat et al. (2016) measured the distribution of silver between copper matte and Fe-spinel saturated FeO<sub>x</sub>-SiO<sub>2</sub> slag at 1200 °C and  $p\text{SO}_2$  of 0.25 atm. However, only a single datum was presented in their study.

Fig. 9(a) indicates that silver preferentially departed into the matte phase and higher matte grades favored the department of silver into matte, as reported previously (Avarmaa et al. 2015). The effects of alumina and lime on the distribution of silver between matte and spinel-saturated iron silicate slag were not evident in the present study. However, it was found in the previous studies (Chen et al. 2021a; Roghani et al. 1997, 2000) that additions of alumina and lime into silica/MgO-saturated iron silicate slags can increase the department of silver into the matte phase. The present logarithmic distribution coefficients of silver between matte and spinel-saturated iron silicate slags fit well with the results by Hidayat et al. (2016) and Roghani et al. (1997) which were obtained at spinel and magnesia saturation, respectively.

The distribution coefficient of nickel in Fig. 9(b) indicates that the partition of nickel favored the matte phase over the entire matte grade range studied. The present distribution coefficients of nickel between matte and spinel-saturated iron silicate slags displayed a somewhat increasing trend with increasing matte grade from 60 to approximately 65–67 wt% Cu, after which they decreased at higher matte grades. The

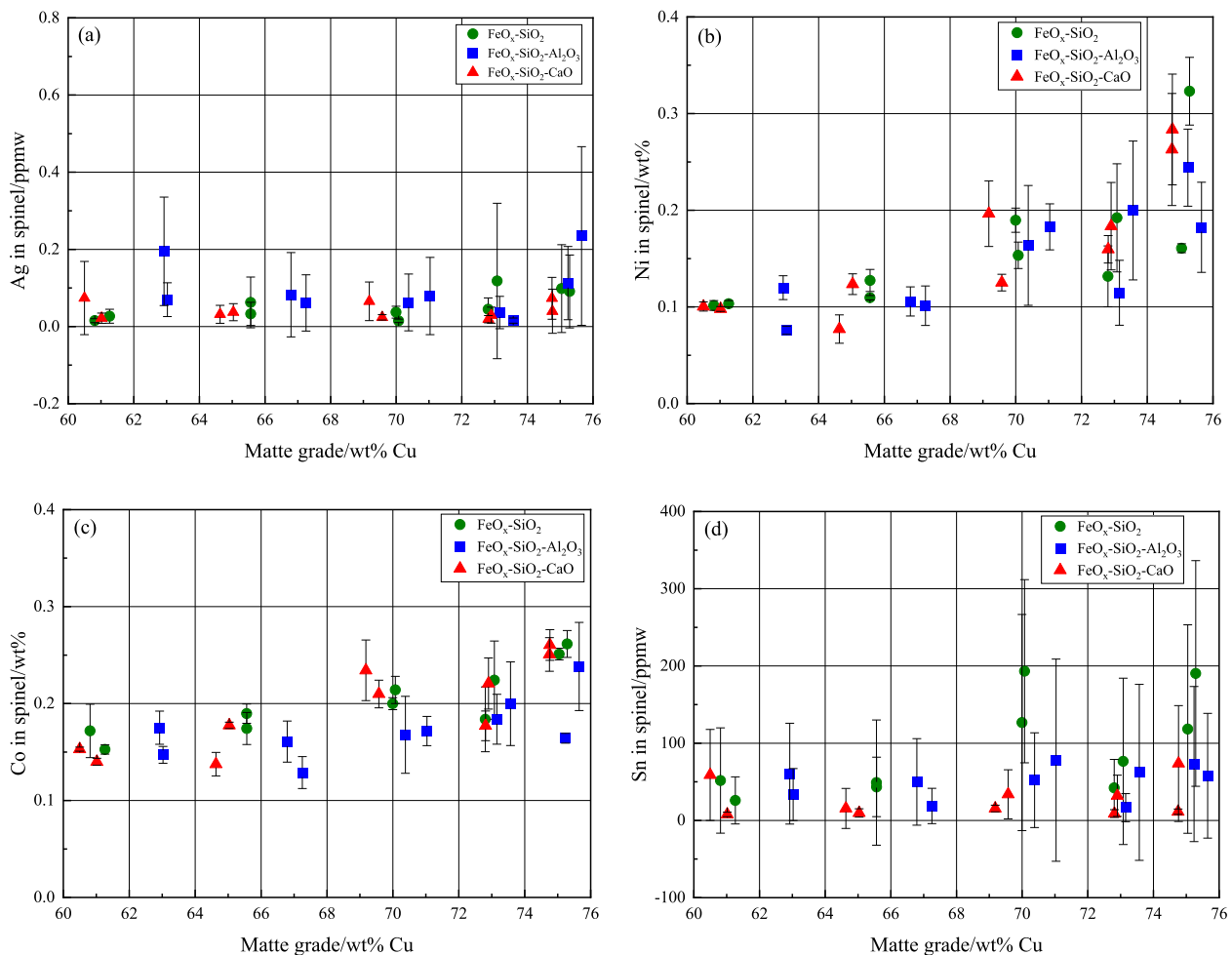


Fig. 8. Concentrations of trace metals in spinel measured by LA-ICP-MS vs matte grade: (a) silver; (b) nickel; (c) cobalt; and (d) tin.

decreasing trends for  $\text{Log}_{10}L^{\text{M/S}}[\text{Ni}]$  were also observed by Chen et al. (2022a) and Yazawa et al. (1983) from spinel and silica saturated samples, respectively. The present results for nickel are in good agreement with the observations by Chen et al. (2022a) but were on the higher side of the data by Yazawa et al. (1983) where bulk analyses of the phases were used. The slag modifiers alumina and lime had little impact on the distribution of nickel between the matte and spinel-saturated iron silicate slag.

As can be seen in Fig. 9(c), the trend lines of the distribution coefficients for cobalt between matte and spinel-saturated iron silicate slags indicate its preference to be deported into the slag phase with increasing matte grade. The present observations for cobalt agreed well with the results by Chen et al. (2022a) and Yazawa et al. (1983). Like the present results for cobalt, the logarithmic distribution coefficients of tin between copper matte and spinel-saturated iron silicate slags displayed decreasing trends with increasing matte grade. The results by Chen et al. (2022a) from spinel-saturated industrial samples and the data by Shishin et al. (2019) and Sukhomlinov et al. (2021) determined between copper matte and silica-saturated iron silicate slag were close to the present results, indicating that the saturation phase did not influence the distribution behavior of tin. The results by Yazawa et al. (1983) displayed similar downward trend with increasing matte grade for tin, although their logarithmic distribution coefficient of tin was about 0.4 log unit higher than the present results, showing predominant accumulation into matte from the condensed phases. Most tin was vaporized in the CO-CO<sub>2</sub>-SO<sub>2</sub>-Ar mixture in the present measurements as the concentration of tin was very low in all phases. The addition of lime into the spinel-saturated iron silicate slag increased the deportment of tin

into matte.

### 3.5. Distribution coefficients between spinel and slag

To have a better understanding about the distribution mechanisms of trace metals in the copper matte smelting system, logarithmic distribution coefficients of the trace metals between spinel and molten slag,  $\text{Log}_{10}L^{\text{Sp/S}}[\text{Me}]$ , were calculated and plotted in Fig. 10 against matte grade.

Silver preferred the molten slag over the spinel phase and the spinel-slag distribution coefficients increased with the increase of matte grade. Additions of alumina and lime into the spinel-saturated iron silicate slag had no obvious impact on the distribution of silver between spinel and slag, similarly as for nickel, cobalt, and tin.

Nickel was slightly enriched in the spinel as a function of matte grade, as seen in Fig. 10(b), as was tin. The distribution coefficient of nickel between spinel and slag increased with increasing matte grade. No significant correlation between the spinel-slag distribution coefficient and matte grade was found for cobalt and tin. For tin, rather significant standard deviations in the spinel phase should be noted. The data reported here are novel and only very limited data for minor element dissolutions in spinel phase can be found from literature.

Combined with the low concentrations of tin in matte, slag, and spinel phases, it can be concluded that tin was mainly vaporized to the gas phase under the present experimental conditions, similar to our previous observations obtained in copper/matte-slag-silica/spinel/wüstite-gas equilibrium systems (Avarmaa et al. 2018; Chen et al. 2021b; Sukhomlinov et al. 2019).

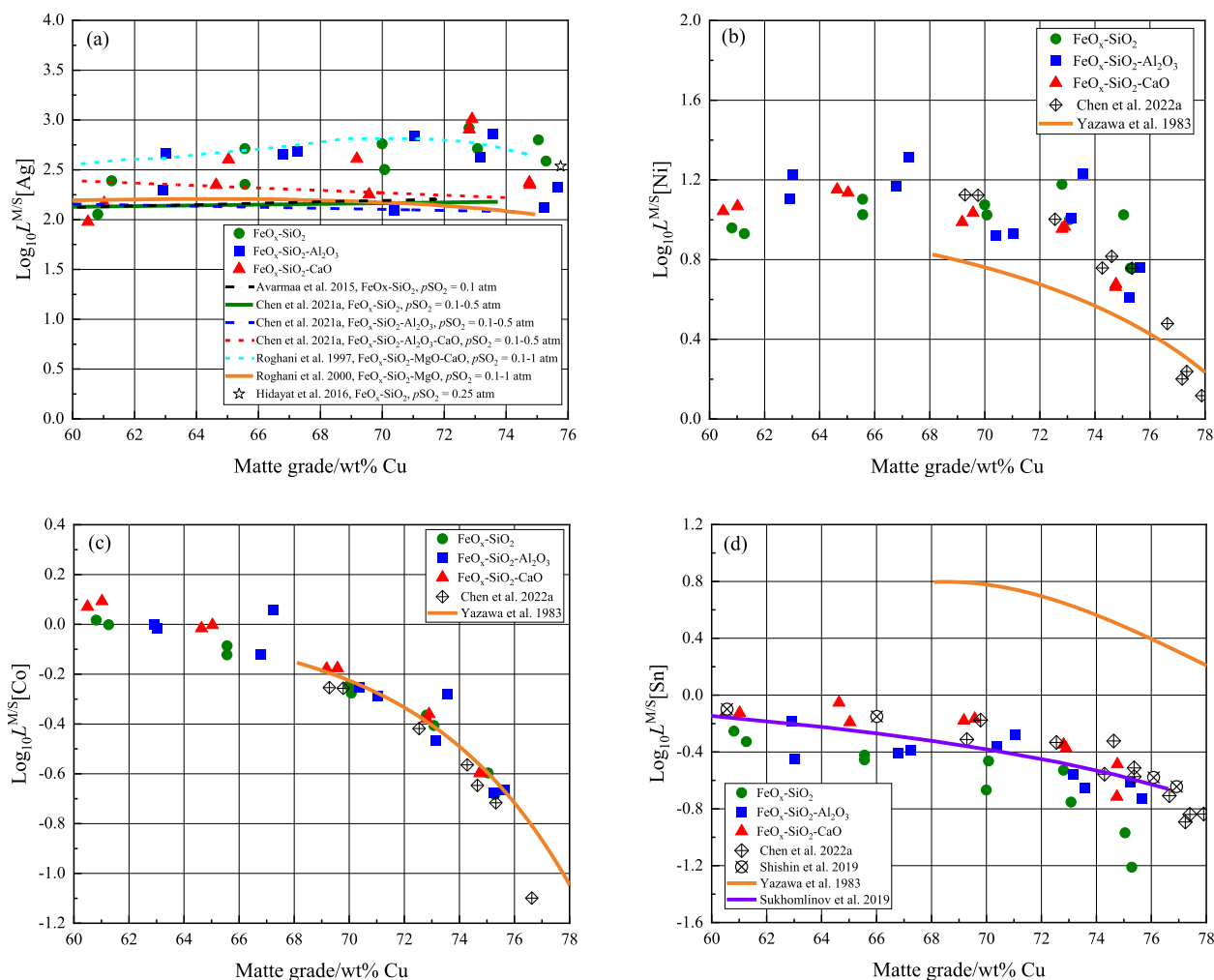


Fig. 9. Logarithmic distribution coefficients of trace metals between matte and spinel-saturated iron silicate slags at 1250 °C and  $p\text{SO}_2$  of 0.25 atm; (a) silver; (b) nickel; (c) cobalt; and (d) tin.

#### 4. Application for industrial practice

Optimal control of the slag chemistry of copper smelting is important for the stable operation of copper smelting processes and at the same time minimizing the loss of copper and other valuable metals in slags (Henao et al. 2010; Mackey 1982; Taskinen 2011). The use of oxygen-enriched air or pure oxygen in modern copper smelting as well as the corrosion of refractory materials resulted in the fact that Fe-spinel (magnetite) is a common phase in cooled copper smelting slags (Chen et al. 2015; Chen et al. 2022a; De Wilde et al. 2016a, 2016b, 2017; Wang et al. 2019). During the oxidation of copper concentrates in the reaction shaft, the magnetite (i.e., the spinel in this study) is formed around the concentrate particles (Hagni et al. 1988; Jun and Zhuo 2018; Jorgensen 1983; Jokilaakso et al. 1991; Pérez-Tello et al. 2018; Stefanova et al. 2004; Taskinen and Jokilaakso 2021).

Thermodynamics of metal distributions are the key for metal recycling through pyrometallurgical processes (Shuva et al. 2016; Taskinen and Avarmaa, 2021). However, limited studies have been carried out for investigating the trace metal distributions between copper/matte and spinel-saturated slags with low slag-to-metal ratios, due to the difficulties of doing experiments in spinel crucibles with aggressive slags. Therefore, the present equilibrium trace metal distribution data provide guidance for accumulating varying trace metals into appropriate phases at low silica concentrations of the slag.

The results described above indicate that the spinel saturation in slag was more beneficial for partitioning silver and nickel into matte than

silica saturation. Moreover, the present observations indicate that the low-silica operation of copper matte smelting and the trace element distribution coefficients are relatively close to those values obtained at silica saturation.

This means that the amounts of trace elements dissolving in the smelting slag are smaller than at silica saturation, due to the smaller slag amount. Therefore, the recoveries of silver and nickel can be effectively improved using the newly proposed fluxing strategy by adding fluxes such as  $\text{Al}_2\text{O}_3$ , MgO, and CaO into slag to adjust the slag properties.

Furthermore, the distribution results for nickel between matte and spinel-saturated slag show that lower matte grades favored the deportment of nickel into matte. Hence, the improvement of the recovery of nickel can be also handled by decreasing matte grade through adjusting the injection of oxygen coefficient of the smelting. Cobalt and tin were preferentially deported into slag/spinel and gas, respectively. Thus, the subsequent slag cleaning and flue dust treatment processes are essential for the recovery of cobalt and tin.

#### 5. Conclusions

The continuously growing slag-to-copper ratio in copper smelting can be cut down only by a radical modification of the operational point in the slag fluxing. A straightforward measure is to lower silica concentration of the slag. As a part of a continuous process for finding more resource efficient smelting and fluxing practices for copper matte smelting and its trace metals recovery from secondary materials, the

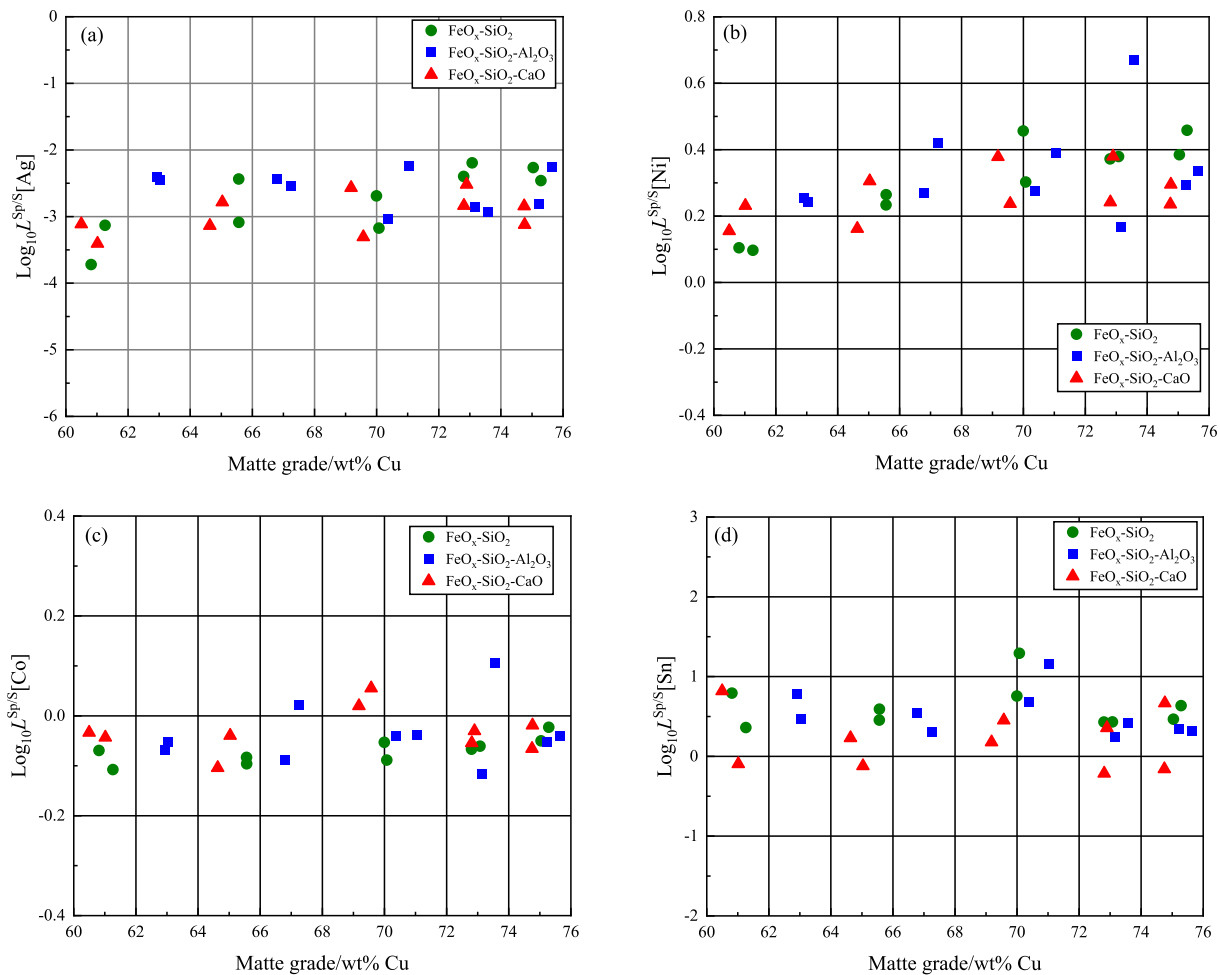


**Fig. 10.** Logarithmic distribution coefficients of trace metals between spinel and spinel-saturated iron silicate slag at 1250 °C and  $p\text{SO}_2$  of 0.25 atm: (a) silver; (b) nickel; (c) cobalt; and (d) tin.

distributions of silver, nickel, cobalt, and tin in the matte-slag-spinel-gas equilibrium were investigated at 1250 °C and  $p\text{SO}_2$  of 0.25 atm by an equilibration and quenching technique. The concentrations of trace metals in matte, slag, and iron spinel at low silica concentrations were measured by combining EPMA and LA-ICP-MS techniques with samples at spinel saturation to avoid the presence of extra substances not belonging to the equilibrium.

Silver and nickel were found to distribute strongly into the sulphide matte rather than into molten slag or spinel. Tin was markedly vaporized into the gas and cobalt deported predominantly into slag and spinel. It was also found that additions of alumina and lime into spinel-saturated iron silicate slag had no significant impact on the distribution coefficients of silver, nickel, and cobalt between matte and slag.

A comparison of the present results determined at spinel saturation and the previous data at silica saturation shows that spinel saturation in slag favored greater department of silver and nickel into matte than at silica saturation. However, the distribution coefficients of cobalt between matte and spinel-saturated iron silicate slags were similar with the observations obtained at silica saturation, indicating that the slag saturation has no major impact on the distributions of cobalt. Moreover, the present distribution coefficients for tin obtained at spinel saturation are similar with previous results (Shishin et al. 2019; Sukhomlinov et al. 2019) determined at silica-saturation and using the similar experimental and analytical techniques but deviate significantly from the observation by Yazawa et al. (1983) using different experimental and analytical methods.

#### CRediT authorship contribution statement

**Min Chen:** Conceptualization, Investigation, Methodology, Software, Data curation, Writing – original draft. **Katri Avarmaa:** Conceptualization, Supervision, Validation, Writing – review & editing. **Pekka Taskinen:** Conceptualization, Software, Supervision, Validation, Writing – review & editing. **Lassi Klemettinen:** Data curation, Writing – review & editing. **Radoslaw Michallik:** Writing – review & editing. **Hugh O'Brien:** Writing – review & editing. **Ari Jokilaakso:** Supervision, Project administration, Resources, Validation, Funding acquisition, Writing – review & editing.

#### Declaration of Competing Interest

The authors declare that they have no known competing financial interests or personal relationships that could have appeared to influence the work reported in this paper.

#### Data availability

Data will be made available on request.

#### Acknowledgments

This study was partly financially supported by Aalto University, School of Chemical Engineering. Min Chen acknowledges the financial support from the China Scholarship Council [number #201806370217].

RAMI (Raw Materials Infrastructure) by Academy of Finland hosted by Aalto University, VTT and GTK at Otaniemi Campus was used in this investigation.

## References

- Avarmaa, K., O'Brien, H., Johto, H., Taskinen, P., 2015. Equilibrium distribution of precious metals between slag and copper matte at 1250–1350 °C. *J. Sustain. Metall.* 1 (3), 216–228. <https://doi.org/10.1007/s40831-015-0020-x>.
- Avarmaa, K., Johto, H., Taskinen, P., 2016. Distribution of precious metals (Ag, Au, Pd, Pt, and Rh) between copper matte and iron silicate slag. *Metall. Mater. Trans. B* 47 (1), 244–255. <https://doi.org/10.1007/s11663-015-0498-4>.
- Avarmaa, K., Yliaho, S., Taskinen, P., 2018. Recoveries of rare elements Ga, Ge, In and Sn from waste electric and electronic equipment through secondary copper smelting. *Waste Manag.* 71, 400–410.
- Bellemans, I., Cnockaert, V., De Wilde, E., Moelans, N., Verbeke, K., 2018a. Metal droplet entrainment by solid particles in slags: an experimental approach. *Journal of Sustainable Metallurgy* 4 (1), 15–32. <https://doi.org/10.1007/s40831-017-0145-1>.
- Bellemans, I., De Wilde, E., Moelans, N., Verbeke, K., 2018b. Metal losses in pyrometallurgical operations—A review. *Adv. Colloid Interface Sci.* 255, 47–63. <https://doi.org/10.1016/j.cis.2017.08.001>.
- Brusselaers, J., Mark, F. E., & Tange, L. (2006). Using metal-rich WEEE plastics as feedstock/fuel substitute for an integrated metals smelter. Technical report produced by PlasticsEurope in cooperation with Umicore and the European Flame Retardants Association. <http://www.plasticseurope.org/> (accessed on 10.03.2022).
- Cesaro, A., Marra, A., Kuchta, K., Belgiorio, V., & Van Hullebusch, E. D. (2018). WEEE management in a circular economy perspective: an overview. *Global NEST J.* 20, 743–750. <https://doi.org/10.30955/gnj.002623>.
- Chen, M., Avarmaa, K., Klemettinen, L., O'Brien, H., Sukhomlinov, D., Shi, J., Taskinen, P., Jokilaakso, A., 2020a. Recovery of precious metals (Au, Ag, Pt, and Pd) from urban mining through copper smelting. *Metall. Mater. Trans. B* 51 (4), 1495–1508. <https://doi.org/10.1007/s11663-020-01861-5>.
- Chen, M., Avarmaa, K., Klemettinen, L., Shi, J., Taskinen, P., Jokilaakso, A., 2020b. Experimental study on the phase equilibrium of copper matte and silica-saturated FeO<sub>x</sub>-SiO<sub>2</sub>-based slags in pyrometallurgical WEEE processing. *Metall. Mater. Trans. B* 51 (4), 1552–1563. <https://doi.org/10.1007/s11663-020-01874-0>.
- Chen, M., Avarmaa, K., Klemettinen, L., Shi, J., Taskinen, P., Lindberg, D., Jokilaakso, A., 2020c. Equilibrium of copper matte and silica-saturated iron silicate slags at 1300 °C and P<sub>SO<sub>2</sub></sub> of 0.5 atm. *Metall. Mater. Trans. B* 51 (5), 2107–2118. <https://doi.org/10.1007/s11663-020-01933-6>.
- Chen, M., Avarmaa, K., Klemettinen, L., O'Brien, H., Shi, J., Taskinen, P., Lindberg, D., Jokilaakso, A., 2021a. Precious metal distributions between copper matte and slag at high P<sub>SO<sub>2</sub></sub> in WEEE reprocessing. *Metall. Mater. Trans. B* 52 (2), 871–882. <https://doi.org/10.1007/s11663-021-02059-z>.
- Chen, M., Avarmaa, K., Taskinen, P., Klemettinen, L., Michallik, R., O'Brien, H., Jokilaakso, A., 2021b. Handling trace elements in WEEE recycling through copper smelting—an experimental and thermodynamic study. *Miner. Eng.* 173, 107189. <https://doi.org/10.1016/j.mineng.2021.107189>.
- Chen, M., Avarmaa, K., Taskinen, P., Michallik, R., Jokilaakso, A., 2022b. An experimental study on the phase equilibria of FeO<sub>x</sub>-saturated iron silicate slags and metallic copper alloys at 1200–1300 °C. *Calphad* 77, 102418. <https://doi.org/10.1016/j.calphad.2022.102418>.
- Chen, M., Cui, Z., & Zhao, B. (2015). Slag chemistry of bottom blown copper smelting furnace at Dongying Fangyuan. In: Jiang, T. (Ed.), 6<sup>th</sup> International Symposium on High-Temperature Metallurgical Processing. Springer, Cham, pp. 257–264. [https://doi.org/10.1007/978-3-319-48217-0\\_33](https://doi.org/10.1007/978-3-319-48217-0_33).
- Chen, M., Avarmaa, K., Taskinen, P., Michallik, R., & Jokilaakso, A. (2022c). Investigation on the matte/slag/spinel/gas equilibria in the Cu-Fe-O-S-SiO<sub>2</sub>-(CaO, Al<sub>2</sub>O<sub>3</sub>) system at 1250 °C and p<sub>SO<sub>2</sub></sub> of 0.25 atm. *Miner. Process. Extractive Metall. Review*, 1–12. In press. <https://doi.org/10.1080/08827508.2022.2047966>.
- Chen, J., Fallah-Mehrjardi, A., Specht, A., O'Neill, H., 2022a. Measurement of minor element distributions in complex copper converting slags using quantitative microanalysis techniques. *JOM* 74 (1), 185–194. <https://doi.org/10.1007/s11837-021-04920-7>.
- Cui, J., Forsberg, E., 2003. Mechanical recycling of waste electric and electronic equipment: a review. *J. Hazard. Mater.* 99 (3), 243–263. [https://doi.org/10.1016/S0304-3894\(03\)00061-X](https://doi.org/10.1016/S0304-3894(03)00061-X).
- Davies, R.H., Dinsdale, A.T., Gisby, J.A., Robinson, J.A.J., Martin, A.M., 2002. MTDATA—thermodynamic and phase equilibrium software from the national physical laboratory. *Calphad* 26 (2), 229–271. [https://doi.org/10.1016/S0364-5916\(02\)00036-6](https://doi.org/10.1016/S0364-5916(02)00036-6).
- De Wilde, E., Bellemans, I., Zheng, L., Campforts, M., Guo, M., Blanpain, B., Moelans, N., Verbeke, K., 2016a. Origin and sedimentation of Cu-droplets sticking to spinel solids in pyrometallurgical slags. *Mater. Sci. Technol.* 32 (18), 1911–1924. <https://doi.org/10.1080/02670836.2016.1151998>.
- De Wilde, E., Bellemans, I., Campforts, M., Guo, M., Blanpain, B., Moelans, N., Verbeke, K., 2016b. Investigation of high-temperature slag/copper/spinel interactions. *Metall. Mater. Trans. B* 47 (6), 3421–3434. <https://doi.org/10.1007/s11663-016-0805-8>.
- De Wilde, E., Bellemans, I., Campforts, M., Guo, M., Vanmeensel, K., Blanpain, B., Moelans, N., Verbeke, K., 2017. Study of the effect of spinel composition on metallic copper losses in slags. *J. Sustain. Metall.* 3 (2), 416–427. <https://doi.org/10.1007/s40831-016-0106-0>.
- Fan, Y., Zhang, B., Song, J., Volski, V., Vandenbosch, G.A., Guo, M., 2018. An innovated application of reutilize copper smelter slag for cement-based electromagnetic interference composites. *Sci. Rep.* 8 (1), 1–6. <https://doi.org/10.1038/s41598-018-34680-5>.
- Gisby, J., Taskinen, P., Pihlasalo, J., Li, Z., Tyrer, M., Pearce, J., Avarmaa, K., Björklund, P., Davies, H., Korpi, M., Martin, S., Pesonen, L., Robinson, J., 2017. MTDATA and the prediction of phase equilibria in oxide systems: 30 years of industrial collaboration. *Metall. Mater. Trans. B* 48 (1), 91–98. <https://doi.org/10.1007/s11663-016-0811-x>.
- Gorai, B., Jana, R.K., 2003. Characteristics and utilisation of copper slag—a review. *Resour. Conserv. Recycl.* 39 (4), 299–313. [https://doi.org/10.1016/S0921-3449\(02\)00171-4](https://doi.org/10.1016/S0921-3449(02)00171-4).
- Hagelüken, C., 2006a. Recycling of electronic scrap at Umicore precious metals refining. *Acta Metall. Slovaca* 12, 111–120.
- Hagelüken, C., 2006b. Recycling of electronic scrap at Umicore's integrated metals smelter and refinery. *Erzmetall* 59 (3), 152–161.
- Hagni, R.D., Vierrether, C.B., Sohn, H.Y., 1988. Process mineralogy of suspended particles from a simulated commercial flash smelter. *Metall. Trans. B* 19 (5), 719–729. <https://doi.org/10.1007/BF02650191>.
- Henao, H.M., Nexhip, C., George-Kennedy, D.P., Hayes, P.C., Jak, E., 2010. Investigation of liquidus temperatures and phase equilibria of copper smelting slags in the FeO-Fe<sub>2</sub>O<sub>3</sub>-SiO<sub>2</sub>-CaO-MgO-Al<sub>2</sub>O<sub>3</sub> system at P<sub>O<sub>2</sub></sub> 10<sup>-8</sup> atm. *Metall. Mater. Trans. B* 41 (4), 767–779. <https://doi.org/10.1007/s11663-010-9369-1>.
- Hidayat, T., Mehrjardi, A. F., Hayes, P. C., & Jak, E. (2016). Experimental study of gas/slag/matte/spinel equilibria and minor elements partitioning in the Cu-Fe-O-S-Si system. In: Reddy R.G., Chaubal P., Pistorius P.C., Pal U. (eds), *Advances in Molten Slags, Fluxes, and Salts: Proceedings of the 10th International Conference on Molten Slags, Fluxes and Salts 2016*. Springer, Cham. pp. 1207–1220. [https://doi.org/10.1007/978-3-319-48769-4\\_130](https://doi.org/10.1007/978-3-319-48769-4_130).
- Jansson, J., Taskinen, P., Kaskiala, M., 2015. Microstructure characterisation of freeze linings formed in a copper slag cleaning slag. *J. Min. Metall. Sect. B* 51 (1), 41–48. <https://doi.org/10.2298/JMMB130320004J>.
- Jokilaakso, A., Suominen, R., Taskinen, P., Lilius, K., 1991. Oxidation of chalcocopyrite in simulated suspension smelting. *Trans. Instit. Min. Metall. (Sect. C: Mineral Processing and Extractive Metallurgy)* 100, C79–C90.
- Jorgensen, F.R., 1983. Single-particle combustion of chalcocopyrite. *Proc. Australasian Instit. Min. Metall.* 288, 37–46.
- Jun, Z., & Zhuo, C. (2018). Smelting mechanism in the reaction shaft of a commercial copper flash furnace. In: Boyd R. Davis et al. (Eds.), *Extraction 2018*. Springer, Cham, 533–546. [https://doi.org/10.1007/978-3-319-95022-8\\_42](https://doi.org/10.1007/978-3-319-95022-8_42).
- Košir, M., Mladenović, A., & Pranjić, A.M., 2021. Applications of copper slag in the construction sector. *Geologica Macedonica*, 35(1), 59–66. <https://doi.org/10.46763/GEOL21351373059mk>.
- Lemouagna, P.N., Yliniemi, J., Adesanya, E., Tanskanen, P., Kinnunen, P., Roning, J., Ilikainen, M., 2020. Reuse of copper slag in high-strength building ceramics containing spodumene tailings as fluxing agent. *Miner. Eng.* 155, 106448. <https://doi.org/10.1016/j.mineng.2020.106448>.
- Lennartsson, A., Engström, F., Samuelsson, C., Björkman, B., Pettersson, J., 2018. Large-scale WEEE recycling integrated in an ore-based Cu-extraction system. *J. Sustain. Metall.* 4 (2), 222–232. <https://doi.org/10.1007/s40831-018-0157-5>.
- Mackey, P.J., 1982. The physical chemistry of copper smelting slags - a review. *Can. Metall. Q.* 21 (3), 221–260. <https://doi.org/10.1179/cmq.1982.21.3.221>.
- Messmann, L., Helbig, C., Thorenz, A., Tuma, A., 2019. Economic and environmental benefits of recovery networks for WEEE in Europe. *J. Clean. Prod.* 222, 655–668. <https://doi.org/10.1016/j.jclepro.2019.02.244>.
- Murari, K., Siddique, R., Jain, K.K., 2015. Use of waste copper slag, a sustainable material. *J. Mater. Cycles Waste Manag.* 17 (1), 13–26. <https://doi.org/10.1007/s10163-014-0254-x>.
- Ogunseit, O.A., Schoenung, J.M., Saphores, J.D.M., Shapiro, A.A., 2009. The electronics revolution: from e-waste to e-waste land. *Science* 326 (5953), 670–671. <https://doi.org/10.1126/science.1176929>.
- Pérez-Tello, M., Parra-Sánchez, V.R., Sánchez-Corralles, V.M., Gómez-Álvarez, A., Brown-Bojórquez, F., Parra-Figueroa, R.A., Balladares-Varela, E.R., Aranedo-Hernández, E. A., 2018. Evolution of size and chemical composition of copper concentrate particles oxidized under simulated flash smelting conditions. *Metall. Mater. Trans. B* 49 (2), 627–643. <https://doi.org/10.1007/s11663-018-1183-1>.
- Phiri, T.C., Singh, P., Nikoloski, A.N., 2021. The potential for copper slag waste as a resource for a circular economy: A review-Part II. *Miner. Eng.* 172, 107150. <https://doi.org/10.1016/j.mineng.2021.107150>.
- Phiri, T.C., Singh, P., Nikoloski, A.N., 2022. The potential for copper slag waste as a resource for a circular economy: A review-Part I. *Miner. Eng.* 180, 107474. <https://doi.org/10.1016/j.mineng.2022.107474>.
- Pouchou, J.L., Pichoir, F., 1986. Basic expression of “PAP” computation for quantitative EPMA. In: Brown, J.D. & Packwood, R.H. (eds.), 11<sup>th</sup> international Congress on X-ray Optics and Microanalysis (ICXOM). Ontario, Canada: Publ. Univ. Western Ontario, pp. 249–253.
- Roghani, G., Hino, M., Itagaki, K., 1997. Phase equilibrium and minor elements distribution between SiO<sub>2</sub>-CaO-FeO<sub>x</sub>-MgO slag and copper matte at 1573 K under high partial pressures of SO<sub>2</sub>. *Mater. Trans. JIM* 38 (8), 707–713. <https://doi.org/10.2320/matertrans1989.38.707>.
- Roghani, G., Takeda, Y., Itagaki, K., 2000. Phase equilibrium and minor element distribution between FeO<sub>x</sub>-SiO<sub>2</sub>-MgO-based slag and Cu<sub>2</sub>S-FeS matte at 1573 K under high partial pressures of SO<sub>2</sub>. *Metall. Mater. Trans. B* 31, 705–712. <https://doi.org/10.1007/s11663-000-0109-9>.
- Shen, H., Forsberg, E., 2003. An overview of recovery of metals from slags. *Waste Manag.* 23 (10), 933–949. [https://doi.org/10.1016/S0956-053X\(02\)00164-2](https://doi.org/10.1016/S0956-053X(02)00164-2).

- Shi, C., Meyer, C., Behnood, A., 2008. Utilization of copper slag in cement and concrete. *Resour. Conserv. Recycl.* 52 (10), 1115–1120. <https://doi.org/10.1016/j.resconrec.2008.06.008>.
- Shishin, D., Hidayat, T., Chen, J., Hayes, P.C., Jak, E., 2019. Combined experimental and thermodynamic modelling investigation of the distribution of antimony and tin between phases in the Cu-Fe-O-S-Si system. *Calphad* 65, 16–24. <https://doi.org/10.1016/j.calphad.2019.01.016>.
- Shuva, M.A.H., Rhamdhani, M.A., Brooks, G.A., Masood, S., Reuter, M.A., 2016. Thermodynamics data of valuable elements relevant to e-waste processing through primary and secondary copper production: a review. *J. Clean. Prod.* 131, 795–809. <https://doi.org/10.1016/j.jclepro.2016.04.061>.
- Stefanova, V., Genevski, K., Stefanov, B., 2004. Mechanism of oxidation of pyrite, chalcocopyrite and bornite during flash smelting. *Can. Metall. Q.* 43 (1), 78–88. <https://doi.org/10.1179/cm.2004.43.1.78>.
- Sukhomlinov, D., Klemettinen, L., O'Brien, H., Taskinen, P., Jokilaakso, A., 2019. Behavior of Ga, In, Sn, and Te in copper matte smelting. *Metall. Mater. Trans. B* 50 (6), 2723–2732. <https://doi.org/10.1007/s11663-019-01693-y>.
- Taskinen, P., 2011. Direct-to-blister smelting of copper concentrates: the slag fluxing chemistry. *Mineral Process. Extractive Metall.* 120 (4), 240–246. <https://doi.org/10.1179/1743285511Y.0000000013>.
- Taskinen, P., Avarmaa, K., 2021. Simulation of slag-matte/metal equilibria for complex and low-grade raw materials. *Sustainability* 13 (22), 12826. <https://doi.org/10.3390/su132212826>.
- Taskinen, P., Jokilaakso, A., 2021. Reaction sequences in flash smelting and converting furnaces: An in-depth view. *Metall. Mater. Trans. B* 52 (5), 3524–3542. <https://doi.org/10.1007/s11663-021-02283-7>.
- Taskinen, P., Kaskiala, M., Hietanen, P., Miettinen, K., Forsström, A., 2011. Microstructure and formation kinetics of a freeze lining in an industrial copper FSF slag. *Mineral Process. Extractive Metall.* 120 (3), 147–155. <https://doi.org/10.1179/1743285511Y.0000000014>.
- Taskinen, P., Kaskiala, M., Miettinen, K., Jansson, J., 2013. Freeze-lining formation and microstructure in a direct-to-blister flash smelting slag. *J. Manuf. Sci. Prod.* 13 (1–2), 77–83. <https://doi.org/10.1515/jmsp-2012-0024>.
- Tesfaye, F., Lindberg, D., Hamuyuni, J., Taskinen, P., Hupa, L., 2017. Improving urban mining practices for optimal recovery of resources from e-waste. *Miner. Eng.* 111, 209–221. <https://doi.org/10.1016/j.mineng.2017.06.018>.
- Van Acherbergh, E., R. C.G., S.E. Jackson, & G. W.L. (2001). Data reduction software for LA-ICP-MS: appendix. P.J. Sylvester (Ed.), *Laser Ablation-ICP-Mass Spectrometry in the Earth Sciences: Principles and Applications*, Mineralog. Assoc. Canada (MAC) Short Course Series, Ottawa, Ontario, Canada, vol. 29, 239–243.
- Wang, J.P., Erdenebold, U., 2020. A study on reduction of copper smelting slag by carbon for recycling into metal values and cement raw material. *Sustainability* 12 (4), 1421. <https://doi.org/10.3390/su12041421>.
- Wang, Q.M., Wang, S.S., Tian, M., Tang, D.X., Tian, Q.H., Guo, X.Y., 2019. Relationship between copper content of slag and matte in the SKS copper smelting process. *Int. J. Miner. Metall. Mater.* 26 (3), 301–308. <https://doi.org/10.1007/s12613-019-1738-4>.
- Yang, T., Zhu, P., Liu, W., Chen, L., Zhang, D., 2017. Recovery of tin from metal powders of waste printed circuit boards. *Waste Manag.* 68, 449–457. <https://doi.org/10.1016/j.wasman.2017.06.019>.
- Yazawa, A., Nakazawa, S., & Takeda, Y., 1983. Distribution behavior of various elements in copper smelting systems. In: Sohn H. Y. et al. (Eds.), *Advances in Sulfide Smelting*, vol. 1. TMS, Warrendale (PA), 99–117.
- Zhang, L., Xu, Z., 2016. A review of current progress of recycling technologies for metals from waste electrical and electronic equipment. *J. Clean. Prod.* 127, 19–36. <https://doi.org/10.1016/j.jclepro.2016.04.004>.
- Zhang, L., Zhou, H., Chen, X., Liu, G., Jiang, C., Zheng, L., 2021. Study of the micromorphology and health risks of arsenic in copper smelting slag tailings for safe resource utilization. *Ecotoxicol. Environ. Saf.* 219, 112321. <https://doi.org/10.1016/j.ecoenv.2021.112321>.
- Zhou, H., Liu, G., Zhang, L., Zhou, C., 2021. Mineralogical and morphological factors affecting the separation of copper and arsenic in flash copper smelting slag flotation beneficiation process. *J. Hazard. Mater.* 401, 123293. <https://doi.org/10.1016/j.jhazmat.2020.123293>.